Modeling production and climate-related impacts on ^{10}Be concentration in ice cores

Christy V. Field,[1] Gavin A. Schmidt,[2] Dorothy Koch,[2] and Colette Salyk[3]

Received 24 June 2005; revised 17 January 2006; accepted 10 April 2006; published 11 August 2006.

[1] The connection between the production of the cosmogenic isotope ^{10}Be and changes in heliomagnetic activity makes ice core ^{10}Be an attractive proxy for studying changes in solar output. However, interpreting ^{10}Be ice core records on centennial timescales is complicated by potential climate-related deposition changes that could obscure the ^{10}Be production signal. By using the Goddard Institute for Space Studies ModelE general circulation model to selectively vary climate and production functions, we model ^{10}Be flux at key ice-coring sites. We vary geomagnetic field strength and the solar activity modulation parameter (ϕ), CO_2, sea surface temperatures, and volcanic aerosols to assess impacts on ^{10}Be. Specifically, we find significant latitudinal differences in the response of ^{10}Be fluxes to changes in the production function. In the climate experiments the ^{10}Be deposition changes simulated over ice sheets in both hemispheres are comparable to those seen in the production experiments. This altered deposition combined with changes of snow accumulation results in significant climate-related ^{10}Be concentration variation in both Greenland and Antarctica. Over the Holocene our results suggest that the ^{10}Be response to climate change should not be neglected when inferring production changes.

Citation: Field, C. V., G. A. Schmidt, D. Koch, and C. Salyk (2006), Modeling production and climate-related impacts on ^{10}Be concentration in ice cores, *J. Geophys. Res.*, *111*, D15107, doi:10.1029/2005JD006410.

1. Introduction

[2] To understand contemporary climate change and anthropogenic climate forcings, it is necessary to quantify solar forcing, the most significant natural forcing on centennial timescales. Sunspot observations go back to 1610, but satellite observations (which span the past 25 years [*Frölich*, 2004]) have greatly increased our understanding of solar activity as it varies over the 11 year sunspot cycle. Despite these advances, the relationship between sunspots and solar activity on multidecadal to centennial timescales, as well as the existence of long-term solar forcing, remains largely speculative [*Foukal et al.*, 2004].

[3] Changes in solar irradiance (defined as the total energy output of the Sun) on the 11 year timescale are positively linked with changes in solar magnetic activity [*Willson and Hudson*, 1988; *Radick et al.*, 1990]. In turn, the Sun's magnetic field modulates galactic cosmic rays (GCR), with increased solar magnetic activity resulting in greater deflection and Earth's reduced exposure to high-energy GCR flux. Collisions between GCR and atmospheric oxygen and nitrogen result in the production of "cosmogenic isotopes" such as ^{10}Be (half-life of 1.5 My), ^{7}Be (half-life 53 days) and ^{14}C (half-life 5730 years) [*Lal and Peters*, 1967; *Masarik and Beer*, 1999]. An anticorrelation therefore exists between ^{10}Be production and solar irradiance, since increased heliomagnetic activity implies both a brighter Sun and diminished ^{10}Be production. These relationships between ^{10}Be production, magnetic activity and solar irradiance are the basis of ^{10}Be's potential use as a proxy for solar activity. However, this chain of influence depends significantly upon the link between the Sun's magnetic field and irradiance changes. Various uncertainties surround these topics and are discussed by *McCracken et al.* [2004], *McCracken* [2004], and *Lean et al.* [2002].

[4] The Earth is also shielded from cosmic rays by its own geomagnetic field, and the combined effect of solar and geomagnetic forces leads to a production function for all cosmogenic isotopes that is stronger in high latitudes than in the tropics, and more pronounced in the stratosphere than in the troposphere [*Lal and Peters*, 1967; *Masarik and Beer*, 1999]. Solar changes impact mainly the high latitudes, while geomagnetic changes affect production closer to the equator.

[5] Beryllium-10 (and ^{7}Be) are produced mainly in the lower stratosphere and upper troposphere; after production, ^{10}Be and ^{7}Be are rapidly scavenged by aerosols (primarily sulfates) [*Lal and Peters*, 1967]. The average residence time in the lower stratosphere is 1 to 2 years [*Davidson et al.*, 1981; *Raisbeck et al.*, 1981b]. Eventually the aerosols descend into the lower troposphere where they are deposited at the surface by both dry (turbulent) and wet (precipitation-related) processes. This quick transition from production to deposition differentiates ^{10}Be from ^{14}C, whose response to

[1]Department of Earth and Environmental Sciences and NASA Goddard Institute for Space Studies, Columbia University, New York, New York, USA.
[2]NASA Goddard Institute for Space Studies and Center for Climate Systems Research, Columbia University, New York, New York, USA.
[3]Division of Geological and Planetary Sciences, California Institute of Technology, Pasadena, California, USA.

0148-0227/06/2005JD006410

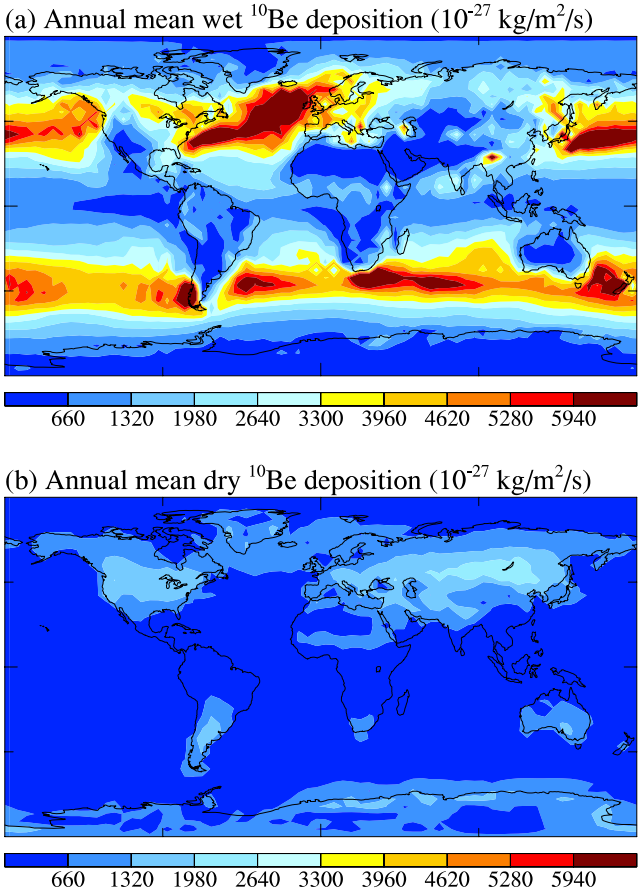

Figure 1. Climatological (a) wet and (b) dry deposition of ^{10}Be from the fixed SST control run.

short-term production changes is significantly damped by the carbon cycle (decreasing ^{14}C's usefulness as an indicator of multidecadal changes in solar activity [*Bard et al.*, 1997]), and whose records may also be affected on centennial timescales by changes in the carbon cycle. In contrast, ^{10}Be's short atmospheric residence time circumvents these complications and leads to high-resolution signals in well-dated polar ice core records [*McHargue and Damon*, 1991].

[6] A complicating factor is the possibility that climatic effects may confound solar signals in the ^{10}Be record [*Lal*, 1987]. Processes that affect the distribution of ^{10}Be in the troposphere, such as changes in stratosphere-troposphere exchange (STE) or aerosol scavenging efficiency, both of which may change with climate, could distort the degree to which ice core records reflect production changes. Similarly, because a more or less active hydrologic cycle may dilute or exaggerate ^{10}Be snow concentrations, any process that affects precipitation (ENSO events [*Brönnimann et al.*, 2004]; changes in thermohaline circulation; long-term changes in the North Atlantic Oscillation/Arctic Oscillation) could also obscure a production rate signal. Figure 1 shows the climatological wet and dry ^{10}Be deposition from one of the control runs (described in the following section), demonstrating the strong link between deposition and precipitation. Midlatitude storm tracks are the dominant regions for wet deposition since the storms, which follow the latitudes associated with high ^{10}Be production, are effective in mixing ^{10}Be-rich air from the stratosphere into the troposphere. Over ice sheets, the magnitude of dry ^{10}Be deposition is comparable to that for wet deposition. It is therefore likely that changes in hydrological and scavenging processes will be linked to changes in ^{10}Be deposition and concentration.

[7] Studies involving ^{10}Be have often used accumulation models [*Cuffey and Clow*, 1997] or oxygen isotope ratios [*Dansgaard et al.*, 1993] to estimate ^{10}Be flux from ice core concentrations. *Finkel and Nishiizumi* [1997] and *Muscheler et al.* [2000] are two examples of such an approach. The main weakness of the concentration-to-flux method is that changes in flux may not necessarily mean that there are also changes in ^{10}Be production; also, it is not always clear whether snow concentration or flux is the most appropriate indicator for changes in atmospheric concentration [*Alley et al.*, 1995]. If ^{10}Be is to be unambiguously used to infer solar variation, we first need a way to account for the effects of climate as they appear in the ice core record; otherwise, it is possible that the coincident variation of climate signals and ^{10}Be snow concentrations may lead to a misattribution of the change to solar forcing. This paper will examine the ways in which production- and climate-related changes impact ^{10}Be deposition. The first experiments to be discussed focus on ^{10}Be's production function and are designed to calibrate how production changes are recorded latitudinally. We also look at simulations involving doubled CO_2 to see how ice core records might change in a warmer climate. Next we examine how ^{10}Be flux responds during periods of reduced North Atlantic Deep Water (NADW) production using two experiments forced with ocean circulation changes. Finally, we look at potential impacts from persistent volcanic eruptions.

2. Goddard Institute for Space Studies ModelE Description

[8] We have used the latest version of the Goddard Institute for Space Studies (GISS) ModelE general circulation model (GCM) [*Schmidt et al.*, 2006]. This version of the model has 20 layers in the vertical and a model top at 0.1 mb. Models with boundaries lower than this have been shown to seriously misrepresent stratosphere-troposphere exchange (STE) and poorly simulate variability in the lower stratosphere [*Rind et al.*, 1999], which may be important in this application. Horizontal resolution is 4° × 5° (latitude × longitude). Tracers are advected, mixed and convected by all processes consistent with the model mass fluxes.

[9] We assume that once produced, beryllium isotopes immediately attach to sulfate aerosols and are 100% soluble. This implies that there are always sufficient sulfate aerosols available to scavenge the ^{10}Be. Aerosol gravitational settling is included, as is a term that allows fine aerosols to settle faster in the stratosphere where the mean free path exceeds the particle radius [*Koch and Rind*, 1998]. In stratiform and convective clouds, aerosol species are transported, dissolved, evaporated and scavenged (with water cloud autoconversion and by raindrop impaction beneath clouds) according to processes for each cloud type. Dissolution of beryllium isotopes is permitted only in proportion to cloud growth, and beryllium evaporation (i.e., the return

Table 1. Model Experiments

Run	Ocean Temperature	Atmosphere	Comments[a]
Control 1	fixed SST	preindustrial GHG	ϕ = 700 MeV, M = 1
Solar minimum	fixed SST	...	ϕ = 500 MeV, M = 1
Geomagnetic minimum	fixed SST	...	ϕ = 700 MeV, M = 0.75
Younger Dryas	fixed SST (no NADW)	...	
8.2 kyr event	fixed SST (60% NADW)	...	
Control 2	mixed layer	...	
2xCO_2	mixed layer	560 ppm CO_2	
Volcanic	mixed layer	1991–2001 volcanic aerosols repeating eruptions	

[a] M, present-day geomagnetic field strength.

of beryllium to the cloud-free portion of the grid box) occurs in proportion to cloud evaporation.

[10] Near the surface, tracers are handled using the same turbulent exchange coefficients as the model humidity. Turbulent dry deposition and interactive surface sources define the surface boundary conditions. The dry deposition scheme is based on the previously used resistance-in-series scheme [*Koch et al.*, 1999] derived from the Harvard GISS chemical transport model [e.g., *Chin et al.*, 1996]; however it is increasingly coupled to the GCM processes, making use of the GCM-assumed leaf area indices, surface types, radiation, boundary layer height, Monin-Obhukov length, etc. A more detailed discussion of the aerosol physics in ModelE can be found by *Koch et al.* [2006].

[11] The different experiments are summarized in Table 1. For all simulations, a 5 year spin-up period was used to ensure that the atmospheric distribution of cosmogenic isotopes had reached equilibrium. When we compared the 5th and 10th years of the control run, the remaining drift in the stratospheric concentration of ^{10}Be was less than 1% per year. The results for the 8.2 kyr event were averaged over 10 years (instead of 5 in the "Younger Dryas" scenario) due to the weak nature of the forcing. For the volcanic experiment, an eruption of aerosols similar to those of the June 1991 Pinatubo eruption was set to take place once per decade. To ensure a robust model response, this simulation was run for 100 years (i.e., 10 eruption cycles).

[12] To simulate the production of ^{10}Be and ^{7}Be, we used the calculated production functions from *Masarik and Beer* [1999] and assumed a control solar modulation parameter of ϕ = 700 MeV. This value is roughly the midpoint between recent solar minimum (400–500 MeV) and maximum (900–1100 MeV) values [*Masarik and Beer*, 1999]. The production function also assumes present-day geomagnetic field strength (M = 1). These parameters result in a mean production rate of about 0.0184 atoms/cm^2 s^1. Other ^{10}Be production rate estimates [*Lal and Peters*, 1967; *Oeschger et al.*, 1970; *O'Brien et al.*, 1978; *Masarik and Reedy*, 1995] exceed that of *Masarik and Beer* [1999] by a factor of 2 or more, which attests to the difficulty of characterizing cosmogenic production in a quantitative manner.

[13] One factor that may explain part of the difference between the *Masarik and Beer* [1999] production function and others is that the Masarik and Beer production function only accounts for ^{10}Be produced by impacts with cosmic ray protons; it does not account for ^{10}Be produced by helium nuclei and heavier nuclei. Although helium and "heavy" nuclei only make up approximately 9% of the incoming cosmic radiation responsible for the production of cosmogenic nuclides (the remaining 91% are protons), these heavier particles are significant since (1) they quickly break up into neutrons and protons, each of which is as effective as a cosmic ray proton at forming ^{10}Be, and (2) their smaller charge/mass ratio makes them more resistant to modulation by changes in geomagnetic and solar magnetic field strength [*McCracken*, 2004]. These conditions imply that the *Masarik and Beer* [1999] production function may underestimate the rate of ^{10}Be production and may slightly overestimate changes in the production rate. However, results for the climate and production change experiments are reported here in terms of percent change from the control runs, which should reduce the significance of potential errors in simulated ^{10}Be production.

3. Model Validation

[14] We used a fixed SST control run to assess the model's performance for unperturbed conditions. As a sensitivity test, we performed a second control run using a 23-layer version with a higher model top [*Schmidt et al.*, 2006], but as results were very similar, we focus exclusively on the 20-layer model. The structure of the production function for ^{7}Be is the same as that for ^{10}Be, but with a different amplitude; since ^{7}Be observations are more plentiful, we use both tracers to help validate the model's ability to simulate beryllium isotopes.

[15] We compared annual mean surface-air ^{7}Be concentrations with observations from 91 locations worldwide; seasonal surface-air ^{7}Be concentrations were also compared with observations from 46 locations worldwide. The Environmental Measurements Laboratory is the primary source for the real-world data (see *Koch et al.* [1996] for references). Also, ^{7}Be observations have been corrected to a mean solar year (as described by *Koch et al.* [1996]) to facilitate their comparison with the control simulations.

[16] Generally, the model does a reasonable job of reproducing the seasonal cycle (Figure 2), including the peaks during spring (due to maximum STE). *Koch et al.* [2006] find that compared to the annual mean data, simulated ^{7}Be surface-air concentrations are sometimes too low, however model values tend to be too high at some high-latitude, Northern Hemisphere locations [see *Koch et al.*, 2006, Figure 2]. High-latitude discrepancies may be due to excessive STE, while the model's overall low bias may be attributed to the production function [*Koch et al.*, 2006], which is low relative to other estimates [*Lal and Peters*,

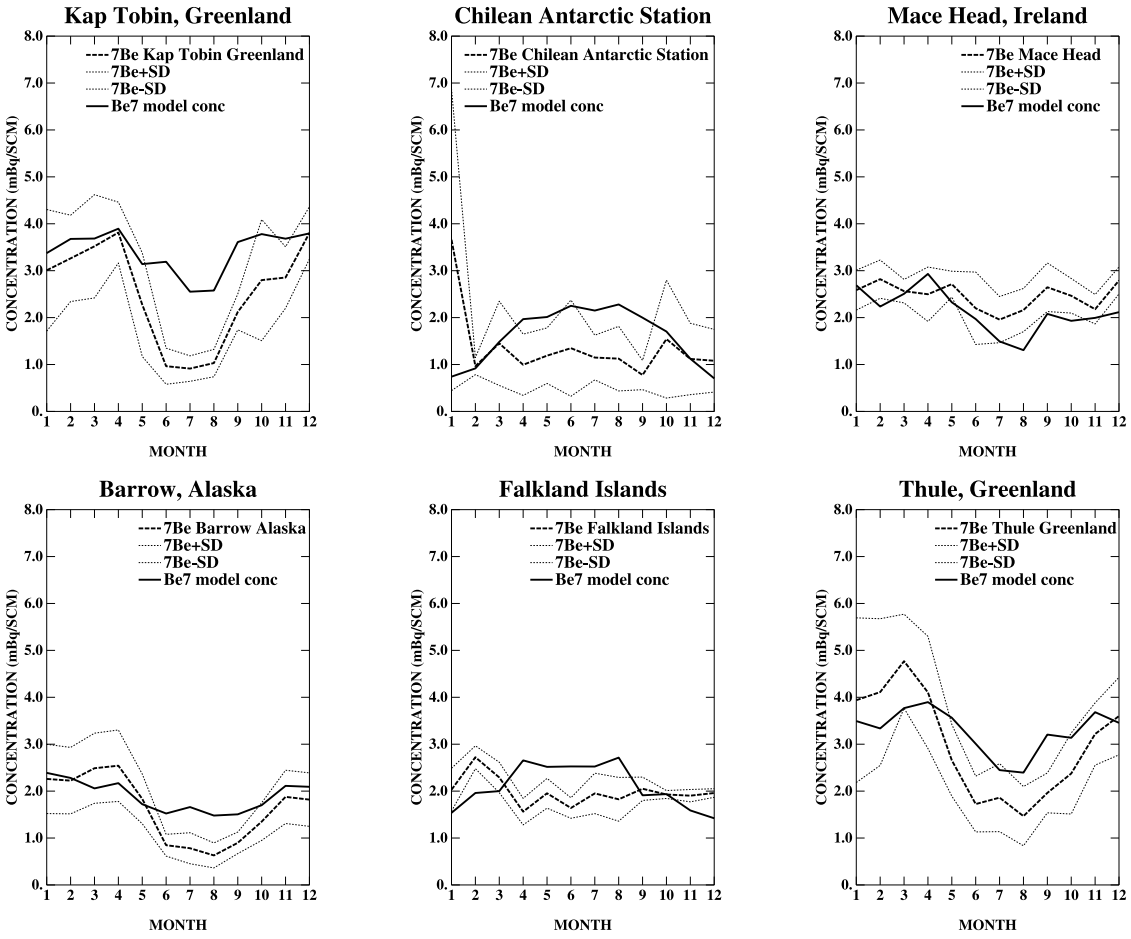

Figure 2. Comparison of seasonal ^{7}Be surface air concentrations with data from the control run. The six sites shown are representative of the model's overall performance. All data are from the Environmental Measurements Laboratory, except for Braunschweig (from *Kolb* [1992]).

1967; *O'Brien et al.*, 1978; *Masarik and Reedy*, 1995]. Comparison between the model and stratospheric aircraft data [see *Koch et al.*, 2006, Figure 17] illustrates the importance of the production function more clearly: at the altitudes associated with ^{7}Be production, the model's atmospheric ^{7}Be concentrations are consistently low (by around a factor of 2) relative to the observations.

[17] We also compare the model to sparser ^{10}Be data. Surface-air observations from the STACCATO project [*Zanis et al.*, 2003] were taken at Jungfraujoch, Switzerland and Zugspitze, Germany (Figure 3). The model is able to

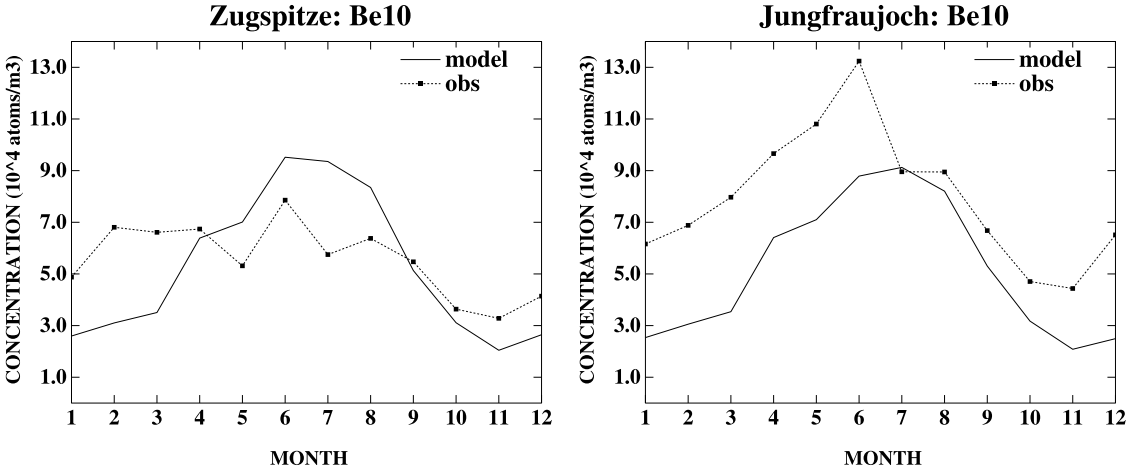

Figure 3. Comparison of seasonal observations of ^{10}Be surface air concentrations [*Zanis et al.*, 2003] from central Europe with output from the control run.

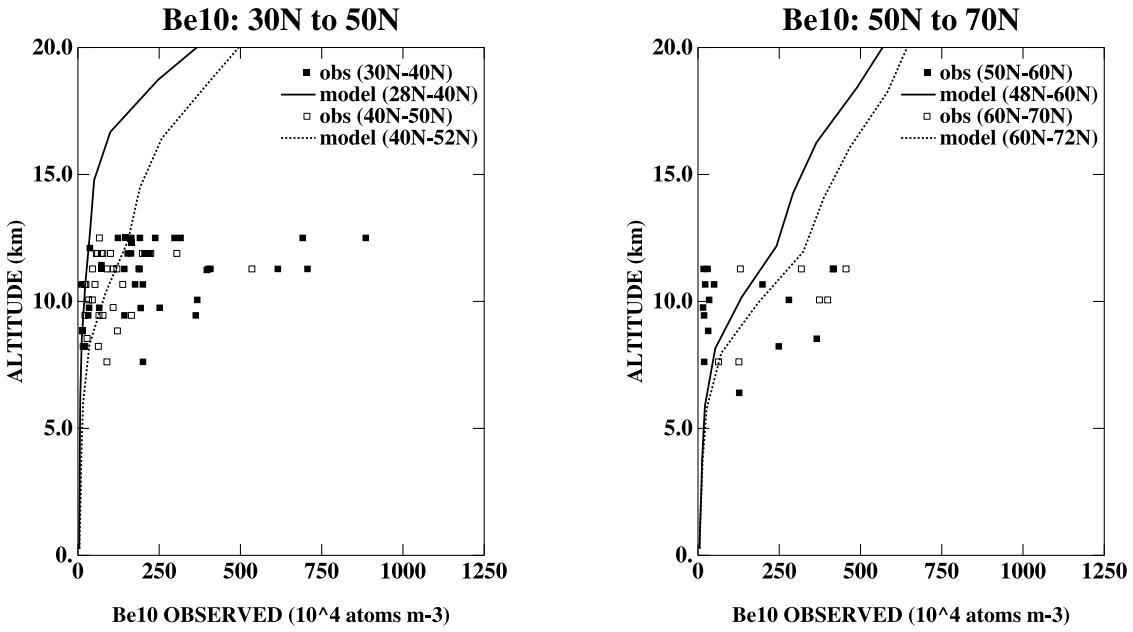

Figure 4. Comparison of middle to high-latitude aircraft ^{10}Be observations [*Jordan et al.*, 2003] with the control run.

capture elements of the seasonal cycles at both locations, although the simulated ^{10}Be is sometimes too low. The data were collected during 2000 and 2001, which were years of relatively high solar activity (ϕ = approximately 860–900 MeV, but 750–900 MeV if the previous years are taken into account due to the effect of the stratospheric residence time) and low ^{10}Be production. The solar modulation was set at 700 MeV in the control run, therefore one would expect simulated ^{10}Be concentrations to be somewhat higher than the observed values. The fact that the opposite is the case suggests once again that the production function is not strong enough.

[18] Surface-air ^{10}Be concentrations at South Pole based on 6 months of data (July–December 1992 (S. Harder, personal communication, 2005)) show values of 3.6×10^4 atoms/m^3, which is smaller than the model's value of 5.2×10^4 atoms/m^3. Sunspot counts for 1990–1992 indicate that the solar modulation varied between approximately 750 and 1100 MeV, which may partly explain why the model's values are higher than the observations. Another contributing factor may be the convergence of the meridians at the South Pole, which is likely to make results for that grid box less representative of Antarctic conditions than data from other Antarctic grid boxes.

[19] Model results were also compared with instantaneous aircraft data collected during 1992 and 1993 for a range of altitudes in the troposphere and stratosphere [*Jordan et al.*, 2003]. Since most samples were taken between 30°N and 70°N, we highlight zonal mean data from this region in Figure 4. The observed values between 40°N and 50°N, though noisy, tend to be somewhat lower than those between 30°N and 40°N; it is not clear why this is the case since ^{10}Be production increases going northward, though it may be a function of local meteorological conditions. From 1992 to 1993, the solar modulation dropped from approximately 750 MeV to 500 MeV. This rapid change, considered along with the high ϕ values in 1990 and 1991, make comparison with the model results more difficult. The agreement between the observations and the model data is also limited by the fact that the observations were taken at a wide range of longitudes while the simulated ^{10}Be values are zonal averages; there is a degree of longitudinal variability associated with planetary wave patterns. That being said, the observed values agree fairly well with the simulated ^{10}Be profiles.

[20] The model's simulation of ^{10}Be snow concentrations at key coring sites is summarized in Table 2. The observed values listed are the approximate values from the top of each core. Because the model has difficulty simulating sufficient accumulation over Summit, control run ^{10}Be snow concentrations are higher than observed (6×10^4 atoms/g in the control run vs. an observed value of approximately 1×10^4 atoms/g [*Yiou et al.*, 1997]). Averaging the control run values of the grid box containing Summit with the two adjacent grid boxes to the east and south barely improves the match (5.2×10^4 atoms/g) despite having a much better snow accumulation. While modeled snow concentrations match observations well at Dye 3, Vostok and Taylor Dome, modeled concentrations are significantly too high at South Pole (consistent with the surface air concentrations mentioned above). One factor that may contribute to the differences between the modeled and observed ^{10}Be snow concentrations is the large uncertainty associated with aerosol scavenging by frozen precipitation. It also is possible that ModelE's tracer transport may contribute somewhat to the discrepancies, however we note that low-altitude poleward transport in the GISS model is more efficient than in other models [*Textor et al.*, 2006]; this appears to improve aerosol distributions at high latitudes [*Koch et al.*, 2006] compared with many previous models [*Rasch et al.*, 2000]. In addition, it is important to acknowledge that the high spatial variability that characterizes

Table 2. Beryllium-10 Snow Concentrations at Ice Core Locations[a]

Run	Summit	Summit Ave.	Dye 3	South Pole	Vostok	Taylor Dome
Observed	~1–2	...	0.5–1	3–4	~9	~2
Control (fixed SST)	6	5.2	1	8.7	12.2	2.9
			Percent Change From Control			
Solar minimum	12.2	12.2	12.2	12.4	12.4	12.4
Geomagnetic minimum	8.3	8.2	8.2	8.1	8.2	8.1
$2xCO_2$	−39 ± 6	−33 ± 9	−12 ± 24	−25 ± 41	−23 ± 11	−44 ± 5
Younger Dryas	68 ± 21	45 ± 16	333 ± 151	6 ± 19	6 ± 13	−10 ± 18
8.2 kyr event	23 ± 98	31 ± 12	35 ± 113	0 ± 80	1 ± 81	−14 ± 70
Peak volcanic	−3 ± 11	−6 ± 3	3 ± 33	19 ± 14	8 ± 12	7 ± 18

[a]Error bars are for one standard deviation (units for observations and control run, 10^4 atoms/g). Values for solar and geomagnetic minimum runs do not have "weather"-related uncertainties because only the tracers were changed in these simulations. Data are from *Yiou et al.* [1997] (Summit), *Beer et al.* [1998] (Dye 3), *Raisbeck and Yiou* [2004] (South Pole), *Raisbeck et al.* [1987] (Vostok), and *Steig et al.* [1998, 2000] (Taylor Dome). Observed concentration values listed here are based on the most topmost data from each core.

Greenland's topography and climate reduces the likelihood that modeled ^{10}Be snow concentrations for a given model grid box will strongly reflect the contents of a particular ice core [*Mosley-Thompson et al.*, 2001]; to a lesser degree, this caveat also applies to the results for Antarctica. The modeled changes in ^{10}Be are therefore less significant at the grid box level and more likely to be useful when considered on a regional scale. Furthermore, looking at the percent change in snow concentration between the control and perturbed runs is a more robust method of assessing the model's performance and is the main way in which results will be described here.

[21] ModelE's ability to realistically simulate a wider, more general range of climate parameters for present-day (1979) conditions is discussed at length by *Schmidt et al.* [2006]. This same paper also describes the model's 20-layer version as having the highest skill relative to two other ModelE configurations (the 23-layer configuration and a 20-layer version with doubled horizontal resolution).

4. Experiments

4.1. Solar and Geomagnetic Experiments

[22] Various studies [*Bard et al.*, 1997; *Steig et al.*, 1996; *Mazaud et al.*, 1994; *McCracken et al.*, 2004; *McCracken*, 2004] have used statistical and mathematical techniques to estimate the degree to which solar and geomagnetic changes are enhanced or suppressed in high-latitude ^{10}Be records while some studies have assumed that there is no latitudinal variation in fluxes [*Muscheler et al.*, 2004a]. In order to assess this, we performed one simulation with reduced geomagnetic field strength (75% of its present-day value) and one simulation with the solar modulation reduced to its approximate value during recent solar minima (ϕ = 500 MeV). Both changes affect global production similarly, about a 10% increase. Geomagnetic changes of this magnitude are expected to take place on millennial timescales, while the simulated solar changes are around a third of the full maximum to minimum range. These simulations are intended to show how production changes might impact ^{10}Be deposition latitudinally, and can be extrapolated for other equilibrium changes.

[23] Figure 5 shows percent change in total ^{10}Be deposition as a function of latitude. The increase in ^{10}Be deposition is not distributed evenly from equator to pole due to the latitudinal difference in production combined with significant mixing across latitudes. Polar deposition in both hemispheres is enhanced by approximately a factor of 1.2 (percent change in polar deposition/percent change in global average deposition) in the solar minimum run and reduced by a factor of 0.8 in the geomagnetic minimum run. These zonal average results are reflected in the model's performance at key coring sites (Table 2).

[24] Our solar value is smaller than the enhancement discussed by *Bard et al.* [1997] (approximately 1.25–2.0, when the ratio is taken as described above), however a correction of their procedure to account for the larger solar modulation for ^{14}C compared to ^{10}Be [*Masarik and Beer*, 1999] implies a slightly smaller range of 1.0–1.6. Our geomagnetic value is very close to the reduction of 0.75 based on observations from Vostok [*Mazaud et al.*, 1994]. Together these results suggest that the expression of geo-

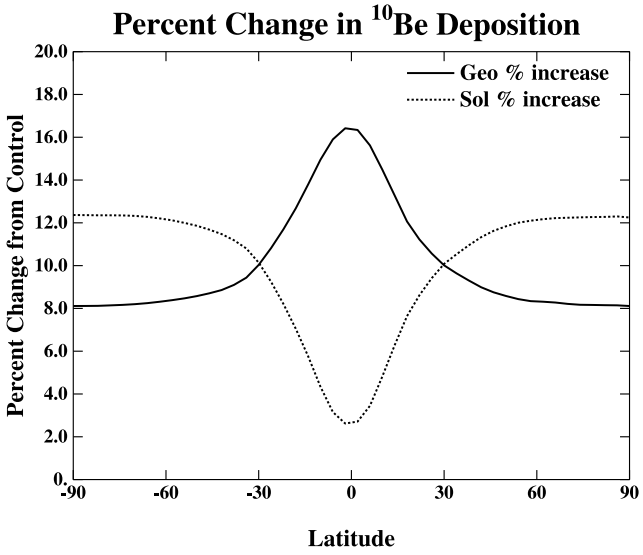

Figure 5. Percent change in total ^{10}Be deposition as a function of latitude. The dotted line shows change in deposition due to reduced solar modulation (ϕ = 500 MeV) compared to ϕ = 700 MeV in the control. The solid line corresponds to deposition change resulting from a 25% decrease in geomagnetic field strength. In both cases, there is a ~10% global mean increase in production (and deposition).

magnetic impacts on ^{10}Be is muted (relative to the global mean) over both polar ice sheet regions, while the effects of solar changes are augmented. Atmospheric mixing of ^{10}Be from lower latitudes to higher latitudes is clearly implicated as in previous results [*Koch and Rind*, 1998], since changes in high-latitude deposition occur despite the fact that the decrease in geomagnetic field strength does not affect ^{10}Be production poleward of approximately 60° latitude [*Masarik and Beer*, 1999]. However, the mixing is not strong enough to remove all latitudinal variation.

4.2. Climate Change Experiments

[25] In the following sections, we look at how climate affects STE and atmospheric ^{10}Be concentrations in the model. We also examine the response of snow accumulation, ^{10}Be deposition and ^{10}Be snow concentration (total dry and wet deposition divided by accumulation) over the Greenland and Antarctic ice sheets. In all of the climate change runs, cosmogenic production functions were kept constant consistent with present-day geomagnetic field strength and mean solar modulation for recent levels of solar activity.

4.2.1. 2xCO$_2$ Experiments

[26] In order to assess the possible climate and transport effects that have influenced ^{10}Be flux during warm periods in the past, we conduct a standard 2xCO$_2$ equilibrium simulation. This allows for a very clear signal-to-noise ratio in the results, and may be compared directly to another similar experiment [*Land and Feichter*, 2003].

[27] For this simulation, we ran the model with a mixed layer ocean (again, keeping ^{10}Be production constant) and compared the results with the mixed layer control run. The atmospheric CO$_2$ concentration in this run is 560 ppm compared to the control value of 280 ppm, giving a global radiative forcing of around 4 W/m^2 and a global mean temperature increase of 2.7°C. In the model, there is greater warming over land masses and over northern North America; also, precipitation increases over the intertropical convergence zone as well as over middle to high northern latitudes and Antarctica. These changes agree qualitatively with those reported in numerous other similar experiments [*Cubasch et al.*, 2001].

[28] *Land and Feichter* [2003] found that, in a warmer climate, the transformed Eulerian mean meridional circulation increases in the stratosphere, while stratospheric ^{10}Be concentrations decrease. In our simulation, stream function values increase between 7% and 35% throughout the stratosphere, implying an intensification of the Brewer-Dobson circulation. Beryllium-7's relatively short half-life (compared to ^{10}Be) can be used to evaluate changes in different loss processes in the warmer climate. Loss of ^{7}Be by decay decreases from 71.1% in the control run to 69.3% in the 2xCO$_2$ run, implying that less ^{7}Be is undergoing radioactive decay in the stratosphere and more ^{7}Be is being transported to the troposphere, where it is deposited at the surface. We also find that concentrations of ^{10}Be (Figure 6) and ^{7}Be (not shown) in the lower stratosphere decrease up to 49% and 33% respectively relative to the control run. These reduced atmospheric concentrations, as well as the changes in stream function and loss by radioactive decay, are all consistent with an increase in the rate of transfer of beryllium isotopes from the stratosphere to the troposphere, similar to the results seen in the previous study.

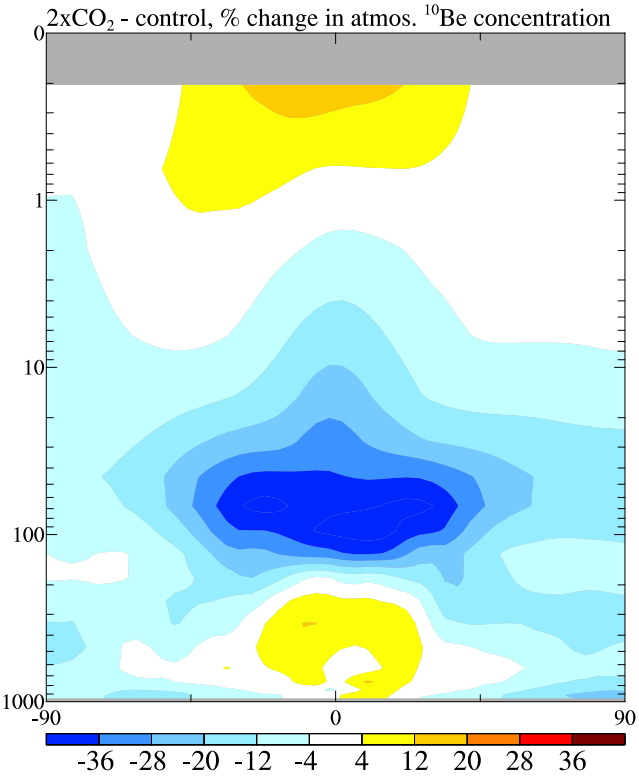

Figure 6. Percent change in atmospheric ^{10}Be concentration for the 2xCO$_2$ simulation relative to the control run (latitude on *x*-axis, pressure in mb on *y*-axis).

[29] The reduced tropospheric ^{10}Be concentrations seen in Figure 6 appear to be due to increased hydrological activity at high latitudes and resulting rainout. Changes in precipitation dominate over deposition changes, which comprise small increases and decreases in total ^{10}Be deposition over Greenland's east and west coasts, respectively. Deposition changes of similar magnitude take place over Antarctica. For both ice sheets, accumulation increases by 10–50%, and ^{10}Be snow concentration drops accordingly by 8–40% (Figures 7a and 7b). Beryllium-10 records during warm climates therefore seem likely to be characterized by a "dilution" effect, with only slight modifications due to changes in deposition.

4.2.2. North Atlantic Ocean Circulation Changes

[30] As a counterpoint to the 2xCO$_2$ simulation, we look at how the ^{10}Be record might change in response to a cooler climate forced by NADW changes. The Younger Dryas (YD) cold event is thought to have been accompanied by an abrupt reduction in NADW production [*Broecker and Denton*, 1990; *Rind et al.*, 2001a, 2001b] and is apparent in the GISP2 ice core from approximately 13 to 11.7 kya. In this core, the YD interval is characterized by a halving of accumulation rate, as well as rapid oxygen isotope and dust concentration changes [*Alley et al.*, 1993]. Beryllium-10 snow concentrations roughly double during this time [*Finkel and Nishiizumi*, 1997], in accordance with the reduced accumulation. The "8.2 kyr event," a period of cooler Northern Hemisphere climate and hypothesized

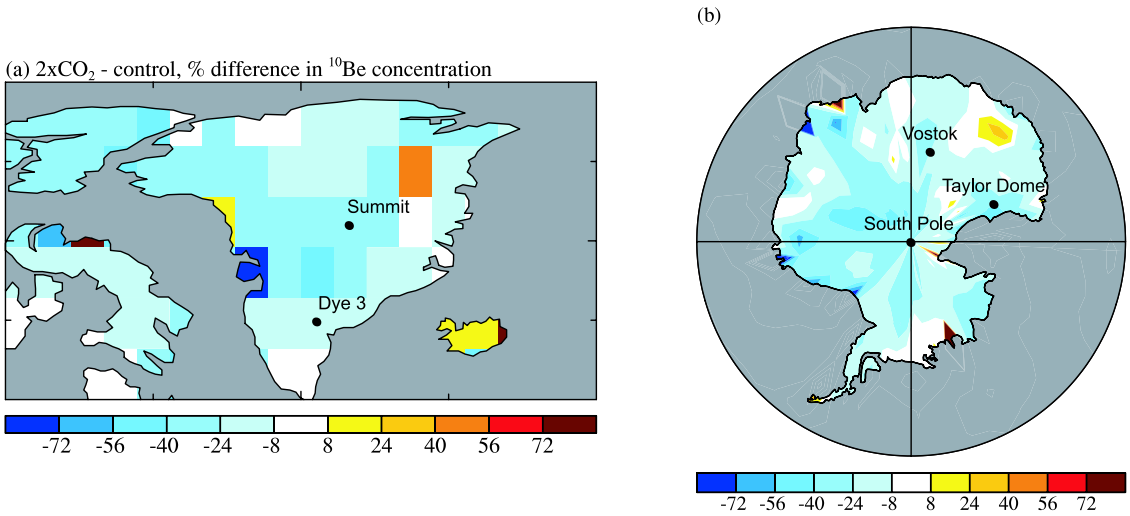

Figure 7. Percent change in ^{10}Be snow concentration for the 2xCO$_2$ simulation relative to the control run.

reduced NADW, is thought to have been caused by the final meltwater pulse from proglacial lakes [*Barber et al.*, 1999]. This event is characterized by approximately a 20% decrease in snow accumulation in the GISP2 record [*Alley et al.*, 1997] and a ^{10}Be snow concentration increase of 38% in the GRIP record. This change was calculated by comparing the average ^{10}Be snow concentration from 8.15 to 8.11 kya (spanning the peak cooling period) with the average concentration from 8.21 to 8.16 kya [*Yiou et al.*, 1997]. New higher-resolution data [*Muscheler et al.*, 2004b] may give a somewhat different result, and so our value should be seen as indicative, rather than definitive.

[31] We simulate the YD and 8.2 kyr event using SST and sea ice parameters fully derived from coupled ocean-atmosphere model simulations of these events. The SST changes for the YD scenario were based on a simulation of complete NADW shutdown [*Rind et al.*, 2001a], resulting in cooler SSTs poleward of 40°N with maximum cooling of 7°–9°C off the southeast coast of Greenland. Northern Hemisphere sea ice increases from 7 to 11% with the greatest increases between 45°N and 75°N. Small sea ice increases (0.6%) also occur around Antarctica. For the 8.2 kyr event, the SST changes were based on the impact of a small meltwater pulse from Lake Agassiz [*LeGrande et al.*, 2006], resulting in a 40% reduction in NADW. The cooling is confined to the north Atlantic with maximum cooling of 1.5°–3.5°C to the south of Greenland. In the Northern Hemisphere, sea ice increases by 2% with the greatest gains in the same latitudes as for the YD; sea ice changes around Antarctica are negligible.

[32] During the YD and the 8.2 kyr events, other climatic changes may have occurred that may or may not have been connected to changes in NADW production, however the changes in climate and ^{10}Be described in this section are based on model runs that are forced only with direct impacts of NADW production changes. Furthermore, the reduced NADW used in our experiments was imposed on a preindustrial climate, which may be substantially different from the actual climates that preceded the YD and the 8.2 kyr event. These factors could therefore impact the applicability of our results, which should only be regarded as the model's response to NADW changes that may be considered characteristic of the YD and 8.2 kyr events.

4.2.2.1. Greenland

[33] The results for Greenland are shown in Figure 8. Results for the 8.2 kyr run are very similar to those for the YD run and are not shown except for changes in ^{10}Be snow concentration. In the YD run, global mean temperature drops 1°C and temperatures over central Greenland drop by 3°–5°C. In the 8.2 kyr run, global mean and Greenland temperature decreases by 0.2°C and 0.5°–1.3°C respectively (about 75% smaller than those in the YD run). Estimates of Greenland cooling associated with the 8.2 kyr event are based on a 1.5–2.0 change in δ^{18}O [*Alley et al.*, 1997; *von Grafenstein et al.*, 1998] and are relatively poorly constrained. The model roughly captures the ratio of the observed estimated Greenland temperature changes (approximately 3:1) between the YD (approximately 15°C cooling [*Johnsen et al.*, 1995; *Schwander et al.*, 1997; *Severinghaus et al.*, 1998]) and 8.2 kyr event (4°–8°C cooling [*Barber et al.*, 1999]), if not the magnitude of the cooling.

[34] The model's lack of success in simulating YD and 8.2 kyr temperatures as cold as those implied by the δ^{18}O records is reflected in the accumulation and ^{10}Be concentration changes for both scenarios. In the YD run, Greenland accumulation decreases by 12–60% while total ^{10}Be deposition increase 5–45% over the northern half of the ice sheet and decreases slightly (5–15%) on the southeast coast. The combined changes in accumulation and deposition result in snow concentration increases greater than 36% over most of eastern Greenland, with a 68% increase at Summit, roughly two-thirds of the observed change of approximately 100% described by *Finkel and Nishiizumi* [1997]. Had the simulated climate over Greenland been colder, it is likely that accumulation would have been further suppressed and snow concentrations would be closer to the observed values.

[35] Similar changes occur in the 8.2 kyr run: accumulation is reduced by 12–60% while total ^{10}Be deposition increases by 2–14% over the southern part of the ice sheet

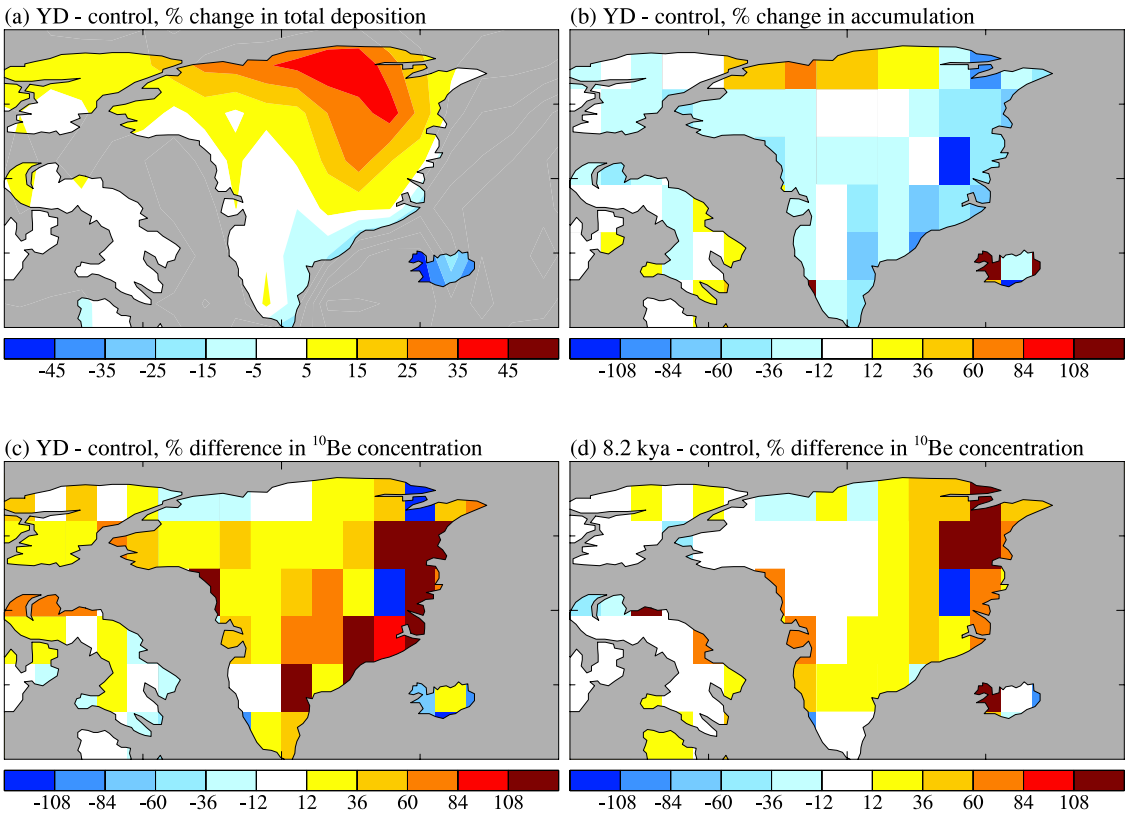

Figure 8. (a) Percent change in total ^{10}Be deposition for the YD simulation. (b) Percent change in accumulation for the YD simulation. (c) Percent change in ^{10}Be snow concentration for the YD simulation. (d) Percent change in ^{10}Be snow concentration for the 8.2 kyr simulation.

and by 2–18% over northern Greenland. These changes lead to ^{10}Be snow concentration increases of 12–60% over most of the central and eastern parts of the continent. The simulated changes in snow concentrations at Summit (23%) are about half as large as the 40% increase observed in the GRIP record.

[36] The apparent explanation for the increased ^{10}Be deposition in these simulations is the cold SST off Greenland's southeastern coast: the cold ocean cools air over the northern North Atlantic, increasing surface pressure and reducing precipitation. As a result, atmospheric ^{10}Be concentrations between 50°N and 90°N increase by 3–21% in the YD (Figure 9) and between 3 and 7% in the 8.2 kyr experiment (not shown). The ^{10}Be-enriched air leads to increased concentrations in wet deposition (snow) and increased dry deposition over Greenland. This increased deposition combines with reduced snow accumulation to produce significantly higher snow concentrations.

[37] To see if transport processes in the YD run might have been affected in a way similar to that seen in the $2xCO_2$ scenario, we looked at changes in stream function, atmospheric concentrations and decay rates. Stream function changes are negligible throughout the stratosphere (±5%). Beryllium-10 concentrations in the stratosphere increase 3–15% compared to the control run (Figure 9), however the percent of ^{7}Be lost to radioactive decay increases only modestly, from 71.1% to 71.7%. Collectively, these results imply that large-scale changes in beryllium advection play a relatively unimportant role in the cold North Atlantic runs.

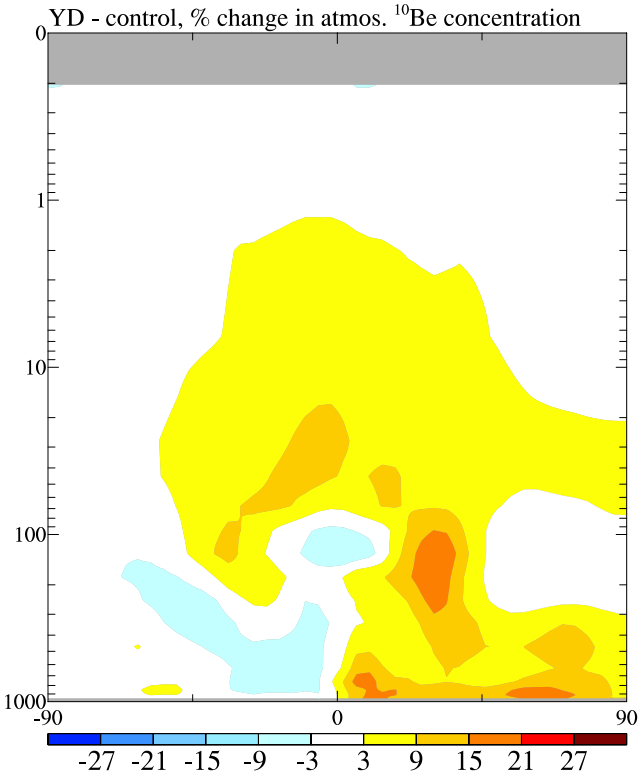

Figure 9. Percent change in atmospheric ^{10}Be concentration for the YD simulation relative to the control run (latitude on *x*-axis, pressure in mb on *y*-axis).

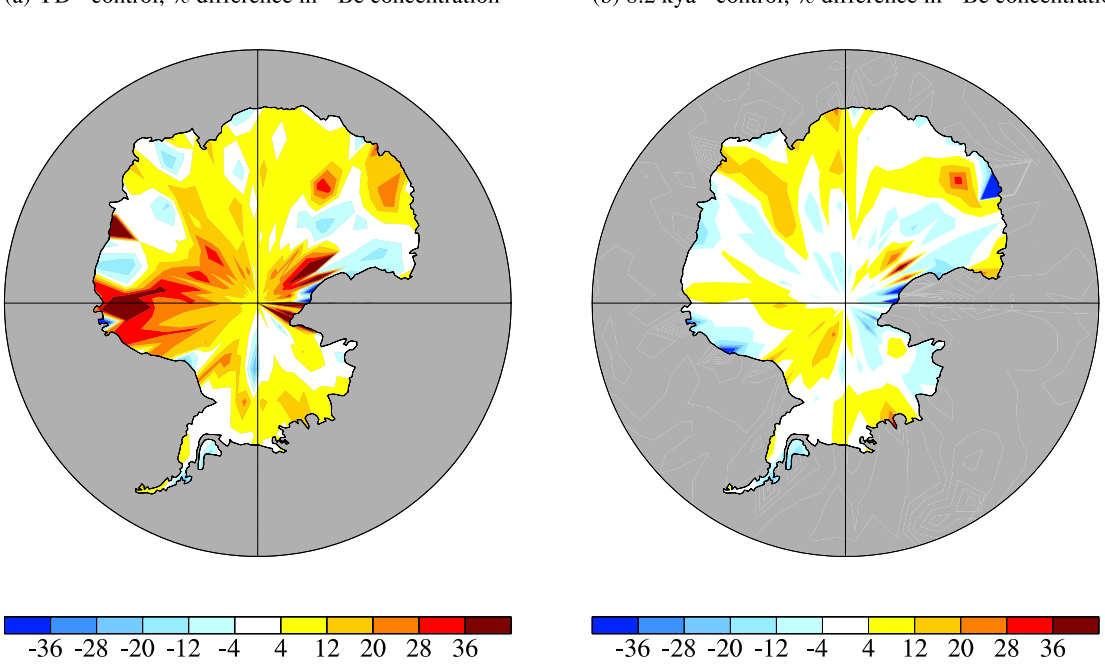

Figure 10. Percent change in ^{10}Be snow concentration for (a) the YD and (b) the 8.2 kyr simulations relative to the control run.

4.2.2.2. Antarctica

[38] Changes similar to those over Greenland take place over Antarctica, though on a smaller scale; the relative magnitudes of the YD and 8.2 kyr changes are however, similar to those over Greenland. Temperatures cool slightly in the YD run, with significant cooling over Dronning Maud Land (1.4°–1.9°C). There are variable increases in ^{10}Be deposition, however accumulation generally decreases (5–35%) due to the cooler temperatures. Consequently, snow concentration increases 5–35% with small regions of higher concentration changes (45% and greater) over parts of Dronning Maud Land and near the Ross ice shelf (Figure 10a). Although ^{10}Be snow concentrations around Taylor Dome decrease in this run, concentrations increase on a larger regional scale. This result is consistent with observations showing that YD ^{10}Be snow concentrations at Taylor Dome exceed preindustrial levels by approximately 100% [*Steig et al.*, 1998], however changes seen in Antarctica may be more directly related to the Antarctic Cold Reversal. We would therefore not expect to capture these changes in a model forced solely with altered NADW production. In the 8.2 kyr run, changes in temperature are not statistically significant, and accumulation and snow concentration changes are smaller and more variable (Figure 10b).

4.2.3. Volcanic Experiments

[39] Explosive volcanic eruptions whose output reaches the stratosphere are typically followed by a period of global cooling due to shortwave absorption and longwave emission of the increased stratospheric aerosol load [*Shindell et al.*, 2003]. Since the residence time for stratospheric aerosols is generally 1 to 2 years, the duration of the aerosol-induced cooling is limited to this timescale. In order to assess whether these short-period events can impact deposition, we analyze data from a 100 year (10-eruption) simulation and compare data from the two coldest years following each eruption (20 years total) with data averaged over the entire simulation. Since we assume that ^{10}Be attaches immediately to sulfate, the increased amounts of stratospheric sulfate resulting from an eruption do not affect the rate of scavenging in our experiments; additionally we do not account for possible reductions in settling time due to the potentially larger size of volcanic sulfates.

[40] In the model, the global mean temperature decreases on average by 0.23°C during the peak cooling period and is associated with a mean radiative forcing over that period of approximately −1.7 W/m^2. Temperatures over Greenland cool by 0.1°–0.4°C and accumulation is reduced over most of Greenland, resulting in a 3–9% decrease in wet ^{10}Be deposition over the southern and northern parts of the ice sheet. There is basically no change in dry deposition, and snow concentration changes are negligible (within ±6% of the 100 year average values). Changes in atmospheric ^{10}Be concentrations and in the transformed Eulerian mean stream function are also within ±6% of average levels (not shown), which implies that any potential STE changes are relatively unimportant.

[41] Similar changes in deposition and temperature take place over Antarctica: temperatures cool 0.1°–0.6°C and accumulation decreases 3–15% over most of the central and eastern parts of the ice sheet. The lowered accumulation is accompanied by reduced wet deposition (2–10% less than the 100 year mean), with negligible changes in dry deposition. However the decreased accumulation has a more dominant effect on snow concentration changes, which increase 5–15% over parts of central and eastern Antarctica (Figure 11), with slightly greater increases at the South Pole (19%). The results collectively suggest that climate changes

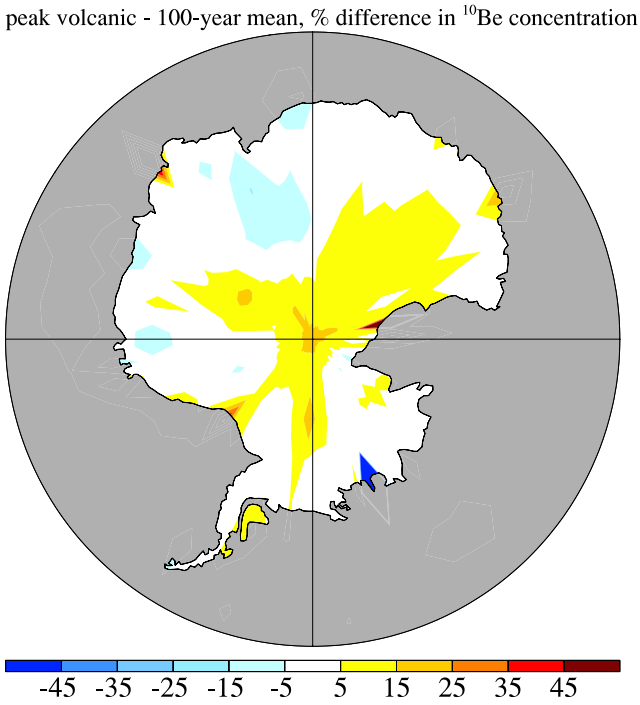

Figure 11. Percent change in ^{10}Be snow concentration for the peak years of the volcanic simulation relative to the 100 year mean.

associated with volcanism are unlikely to impact Greenland ^{10}Be records significantly, but may have a more variable impact on Antarctic records.

5. Conclusions

[42] Model simulations using beryllium isotope tracers were performed to see how changes in production function and climate may impact ^{10}Be flux over polar ice-coring areas. In the production change experiments, a lower level of solar activity enhances polar ^{10}Be deposition relative to global average deposition (or production) by a factor of 1.2; reduced geomagnetic activity lowers polar ^{10}Be deposition by a factor of 0.8. Both values are similar to those inferred in earlier studies [*Bard et al.*, 1997; *Mazaud et al.*, 1994]. When interpreting ice core records, however, one must bear in mind the timescales typically associated with production-related changes: ^{10}Be enhancement associated with geomagnetic changes is more likely to present itself as a long-term trend extending over centuries or millennia, while solar changes such as those related with Spörer and Maunder minima appear to take place over multidecadal to centennial timescales.

[43] In both of the reduced NADW experiments (YD and 8.2 kyr event), the model simulates ^{10}Be snow concentration increases at Summit that are roughly half those seen in the ice core record, possibly consistent with the underestimated temperature response in Greenland. The modeled increases in both snow concentrations and atmospheric concentrations are accomplished without any change in solar modulation, implying that the observed changes may not be indicative solely of a solar-forced response [*Muscheler et al.*, 2004b]. We also note the relatively linear change in ^{10}Be snow concentrations between the YD and 8.2 kyr scenarios, which suggests that while concentration changes seen during the YD are significant, they should not necessarily be considered the anomalous result of a large-scale climate shift, but rather part of a continuum that also encompasses the changes seen in the 8.2 kyr simulation.

[44] In the runs with radiative forcings, changes in ^{10}Be snow concentrations are dominated by changes in precipitation: warming in the $2xCO_2$ run leads to a dilution of ^{10}Be over ice sheets, and cooling in the volcanic run leads to lower precipitation and higher snow concentrations. The $2xCO_2$ run is characterized by competing increases in both STE and precipitation, demonstrating that increased stratospheric transport does not necessarily translate into increased ^{10}Be snow concentration. Conversely, changes in snow concentration are not always linked to changes in STE, as shown in the YD simulation.

[45] Snow concentration changes over Antarctica appear to be roughly scalable to the degree of radiative forcing. In the volcanic run, the forcing is approximately -1.7 W/m^2 and Antarctic ^{10}Be snow concentrations increase by 5–15%. In the $2xCO_2$ run, the radiative forcing is approximately 4 W/m^2 and snow concentrations decrease by 8–40%. These results suggest a tentative rule of thumb of approximately a 10% change in Antarctic snow concentration for every 1 W/m^2 of forcing. The more variable nature of Greenland's climate is the most likely cause for its exclusion from this relationship.

[46] Changes in radiative forcing from roughly 1850 to the present have been around 1.6 ± 1 W/m^2 (of which approximately 0.8 W/m^2 has not yet been realized [*Hansen et al.*, 2005]). Temperature change has been around 0.8°C, which is approximately 30% of the change seen in equilibrium $2xCO_2$ runs. Thus it is conceivable that concentration changes of ~10% may have occurred as a result of 20th century climate change. We stress, however, that this remains to be demonstrated in full 20th century transient experiments. More work is required to understand responses over both ice sheets under various conditions, and to assess the strength of any potential link between snow concentration and radiative forcing in general.

[47] Over the course of the 11 year solar cycle, ^{10}Be snow concentration changes by roughly ±10–20% relative to the concentration during an average solar year (or a 40% decrease from minimum to maximum) [*McCracken et al.*, 2004; *Steig et al.*, 1996]. This response is mostly larger than the concentration changes seen in the climate perturbation experiments. However on centennial timescales, ^{10}Be's response to longer-term solar variability may be more comparable to the synchronous climate-related concentration changes. These considerations make it more difficult to ascribe specific causes to changes in the ^{10}Be ice core record, and in particular to distinguish between climate-related and solar-related changes. Furthermore, if changes in solar output are accompanied by changes in the solar magnetic field, then a less active Sun is likely to result not only in increased ^{10}Be production, but also in climate changes that may significantly enhance the (already heightened) ^{10}Be snow concentrations over ice sheet regions. Interpreting the ^{10}Be record without accounting for possible climate-related changes carries the risk of inferring the

existence of solar changes that are larger than those which actually occurred.

[48] These results illustrate the potential difficulty of ascribing specific causes to changes in the ^{10}Be ice core record, and in particular of distinguishing between climate-related and solar-related changes. For example, if we assume that changes in solar output will be accompanied by changes in the solar magnetic field, then a less active Sun is likely to result not only in increased ^{10}Be production, but also in climate changes that may significantly enhance the (already heightened) ^{10}Be snow concentrations over ice sheet regions. Interpreting the ^{10}Be record without accounting for possible climate-related changes carries the risk of inferring the existence of solar changes that are larger than those which actually occurred.

[49] One time period of particular interest is the Maunder Minimum (late 17th century) during which ^{10}Be snow concentrations increased by ~50% at Dye 3 and ~40% at the South Pole (1690–1710 CE compared to 1730–1750 CE) [*Bard et al.*, 1997; *McCracken et al.*, 2004]. Reduced sunspot activity and increased volcanism most likely contributed to significant global cooling at this time. *McCracken et al.* [2004] estimate that this period was characterized by values for ϕ as low as 84 MeV, which correspond approximately to a 40% increase in global mean ^{10}Be production relative to average present-day conditions. However, accounting for the cooler climate and the impact of solar activity (including the response of ozone to UV variability and related dynamic effects [*Shindell et al.*, 1999]) may imply that some fraction of the ^{10}Be change was climatic. In future work, we hope to be able to improve the calibration of ^{10}Be by examining the combined effects of climate and production-related changes both during the Maunder Minimum and over the course of the 11 year solar cycle.

[50] The results presented here are also relevant for longer-term variability. During the last 10 ky, ^{10}Be snow concentrations at Summit and the South Pole vary from the mean values by up to approximately ±45% [*Finkel and Nishiizumi*, 1997; *Yiou et al.*, 1997; *Raisbeck et al.*, 1981a] on centennial timescales. Given that there have been significant changes in greenhouse gases, volcanism and North Atlantic circulation changes over this period, the associated climatically forced ^{10}Be snow concentration changes could therefore be significant. Further investigation of specific time periods with more clearly defined forcings will be required to better quantify this relationship.

[51] **Acknowledgments.** We would like to thank Jürg Beer and Josef Masarik for supplying ^{10}Be and ^{7}Be production functions and Podromos Zanis for providing the STACCATO data. We also thank Carolyn Jordan for supplying the ^{10}Be aircraft data and Susan Harder for allowing access to unpublished South Pole data. Many thanks to EML/HASP (http://www.eml.st.dhs.gov/databases/hasp) and EML/SASP (http://www.eml.st.dhs.gov/databases/sasp) for providing the observed ^{7}Be data. Raimund Muscheler and two anonymous reviewers helped improve the manuscript substantially. Support for this project was provided by NSF grant ATM-0317562. C.F. also acknowledges support from the U.S. National Science Foundation through a Fellowship in the IGERT Joint Program in Applied Mathematics and Earth and Environmental Sciences at Columbia University.

References

Alley, R. B., et al. (1993), Abrupt increase in Greenland snow accumulation at the end of the Younger Dryas event, *Nature*, *362*, 527–529.

Alley, R. B., R. C. Finkel, K. Nishiizumi, A. Anandakrishnan, C. A. Shuman, G. R. Mershon, G. A. Zielinski, and P. A. Mayewski (1995), Changes in continental sea-salt atmospheric loadings in central Greenland during the most recent deglaciation: Model based estimates, *J. Glaciol.*, *41*, 503–514.

Alley, R. B., P. A. Mayewski, T. Sowers, M. Stuiver, K. C. Taylor, and P. U. Clark (1997), Holocene climatic instability: A prominent, widespread event 8200 yr ago, *Geology*, *25*, 483–486.

Barber, D. C., et al. (1999), Forcing of the cold event of 8,200 years ago by castastrophic drainage of Laurentide lakes, *Nature*, *400*, 344–348.

Bard, E., G. M. Raisbeck, F. Yiou, and J. Jouzel (1997), Solar modulation of cosmogenic nuclide production over the last millennium: Comparison between ^{14}C and ^{10}Be records, *Earth Planet. Sci. Lett.*, *150*, 453–462.

Beer, J., S. Tobias, and N. Weiss (1998), An active Sun throughout the Maunder minimum, *Sol. Phys.*, *181*, 237–249.

Broecker, W. S., and G. H. Denton (1990), The role of ocean-atmosphere reorganizations in glacial cycles, *Quat. Sci. Rev.*, *9*, 305–341.

Brönnimann, S., J. Luterbacher, J. Staehelin, T. Svendby, G. Hansen, and T. Svoe (2004), Extreme climate of the global troposphere and stratosphere in 1940–42 related to El Niño, *Nature*, *431*, 971–974.

Chin, M., D. J. Jacob, G. M. Gardner, M. S. Foreman-Flower, P. A. Spiro, and D. L. Savoie (1996), A global three-dimensional model of tropospheric sulfate, *J. Geophys. Res.*, *101*, 18,667–18,690.

Cubasch, U., G. Meehl, G. Boer, R. Stouffer, M. Dix, A. Noda, C. Senior, S. Raper, and K. Yap (2001), Projections of future climate change, in *Climate Change, 2001: The Scientific Basis, Contribution of Working Group 1 to the Third Assessment Report of the Intergovernmental Panel on Climate Change*, edited by J. Houghton et al., pp. 525–582, Cambridge Univ. Press, New York.

Cuffey, K. M., and G. C. Clow (1997), Temperature, accumulation, and ice sheet elevation in central Greenland through the last deglacial transition, *J. Geophys. Res.*, *102*, 26,383–26,396.

Dansgaard, W., et al. (1993), Evidence for general instability of past climate from a 250-kyr ice-core record, *Nature*, *364*, 218–330.

Davidson, C. L., T. C. Chu, M. A. Grimm, N. A. Nasta, and M. P. Qamoos (1981), Wet and dry deposition of trace elements onto the Greenland ice sheet, *Atmos. Environ.*, *15*, 1429–1437.

Finkel, R. C., and K. Nishiizumi (1997), Beryllium-10 concentrations in the Greenland Ice Sheet Project 2 ice core from 3–40 ka, *J. Geophys. Res.*, *102*, 26,699–26,706.

Foukal, P., G. North, and T. Wigley (2004), A stellar view on solar variations and climate, *Science*, *306*, 68–69.

Fröhlich, C. (2004), Solar irradiance variability, in *Solar Variability and Its Effect on Climate*, *Geophys. Monogr. Ser.*, vol. 141, edited by J. M. Pap and P. Fox, pp. 97–110, AGU, Washington, D. C.

Hansen, J., et al. (2005), Earth's energy imbalance: Confirmation and implications, *Science*, *308*, 1431–1435.

Johnsen, S. J., D. Dahl-Jensen, W. Dansgaard, and N. Gundestrup (1995), Greenland paleotemperatures derived from GRIP core hole temperature and ice isotope profiles, *Tellus, Ser. B*, *47*, 624–629.

Jordan, C. E., J. E. Dibb, and R. C. Finkel (2003), ^{10}Be/^{7}Be tracer of atmospheric transport and stratosphere-troposphere exchange, *J. Geophys. Res.*, *108*(D8), 4234, doi:10.1029/2002JD002395.

Koch, D. M., and D. Rind (1998), Beryllium 10/beryllium 7 as a tracer of stratospheric transport, *J. Geophys. Res.*, *103*, 3907–3917.

Koch, D. M., D. J. Jacob, and W. C. Graustein (1996), Vertical transport of aerosols in the troposphere as indicated by ^{7}Be and ^{210}Pb in a chemical tracer model, *J. Geophys. Res.*, *101*, 18,651–18,666.

Koch, D., D. Jacob, I. Tegen, D. Rind, and M. Chin (1999), Tropospheric sulfur simulation and sulfate direct radiative forcing in the Goddard Institute for Space Studies general circulation model, *J. Geophys. Res.*, *104*, 23,799–23,822.

Koch, D., G. A. Schmidt, and C. V. Field (2006), Sulfur, sea salt, and radionuclide aerosols in GISS ModelE, *J. Geophys. Res.*, *111*, D06206, doi:10.1029/2004JD005550.

Kolb, W. (1992), Aktivitatskonzentrationen von Radionukliden in der bodennahen Luft Norddeutschlands und Nordnorwegens im Zeitraum von 1963 bis 1990, *Rep. Ra-29*, Phys. Tech. Bundesanst, Braunschweig, Germany.

Lal, D. (1987), ^{10}Be in polar ice: Data reflect changes in cosmic ray flux or polar meteorology, *Geophys. Res. Lett.*, *14*, 785–788.

Lal, D., and B. Peters (1967), Cosmic ray produced radioactivity on the Earth, *Handb. Phys.*, *46*, 551–612.

Land, C., and J. Feichter (2003), Stratosphere-troposphere exchange in a changing climate simulated with the general circulation model MAECHAM4, *J. Geophys. Res.*, *108*(D12), 8523, doi:10.1029/2002JD002543.

Lean, J. L., Y.-M. Wang, and N. R. Sheeley Jr. (2002), The effect of increasing solar activity on the Sun's total and open magnetic flux during multiple cycles: Implications for solar forcing of climate, *Geophys. Res. Lett.*, *29*(24), 2224, doi:10.1029/2002GL015880.

LeGrande, A. N., G. A. Schmidt, D. T. Shindell, C. Field, R. L. Miller, D. Koch, G. Faluvegi, and G. Hoffman (2006), Consistent simulations of multiple proxy responses to an abrupt climate change event, *Proc. Natl. Acad. Sci. U. S. A.*, *103*, doi:10.1073/pnas.0510095103.

Masarik, J., and J. Beer (1999), Simulation of particle fluxes and cosmogenic nuclide production in the Earth's atmosphere, *J. Geophys. Res.*, *104*, 12,099–12,111.

Masarik, J., and R. C. Reedy (1995), Terrestrial cosmogenic-nuclide production systematic calculated from numerical simulations, *Earth Planet. Sci. Lett.*, *136*, 381–395.

Mazaud, A., C. Laj, and M. Bender (1994), A geomagnetic chronology for Antarctic ice accumulation, *Geophys. Res. Lett.*, *21*, 337–340.

McCracken, K. G. (2004), Geomagnetic and atmospheric effects upon the cosmogenic ^{10}Be observed in polar ice, *J. Geophys. Res.*, *109*, A04101, doi:10.1029/2003JA010060.

McCracken, K. G., F. B. McDonald, J. Beer, G. Raisbeck, and F. Yiou (2004), A phenomenological study of the long-term cosmic ray modulation, 850–1958 AD, *J. Geophys. Res.*, *109*, A12103, doi:10.1029/2004JA010685.

McHargue, L. R., and P. E. Damon (1991), The global beryllium 10 cycle, *Rev. Geophys.*, *29*, 141–158.

Mosley-Thompson, E., J. R. McConnell, R. C. Bales, Z. Li, P.-N. Lin, K. Steffen, L. G. Thompson, R. Edwards, and D. Bathke (2001), Local to regional-scale variability of annual net accumulation on the Greenland ice sheet from PARCA cores, *J. Geophys. Res.*, *106*, 33,839–33,851.

Muscheler, R., J. Beer, G. Wagner, and R. C. Finkel (2000), Changes in deep-water formation during the Younger Dryas event inferred from ^{10}Be and ^{14}C records, *Nature*, *408*, 567–570.

Muscheler, R., J. Beer, P. W. Kubik, and H.-A. Synal (2004a), Geomagnetic field intensity during the last 60,000 years based on ^{10}Be and ^{36}Cl from the summit ice cores and ^{14}C, *Quat. Sci. Rev.*, *24*, 1849–1860.

Muscheler, R., J. Beer, and M. Vonmoos (2004b), Causes and timing of the 8200 yr BP event inferred from the comparison of the grip ^{10}Be and the tree ring ^{14}C record, *Quat. Sci. Rev.*, *23*, 2101–2111.

O'Brien, K., H. A. Sandmeier, G. Hansen, and J. E. Campbell (1978), Cosmic ray induced neutron background sources and fluxes for geometries of air over water, ground, iron, and aluminum, *J. Geophys. Res.*, *83*, 114–120.

Oeschger, H., J. Houtermann, H. Loosli, and M. Wahlen (1970), The constancy of cosmic radiation from isotope studies in meteorites and on the Earth, in *Radiocarbon Variations and Absolute Chronology*, edited by I. Olsen, pp. 471–498, John Wiley, Hoboken, N. J.

Radick, R. R., G. W. Lockwood, and S. L. Baliunas (1990), Stellar activity and brightness variations: A glimpse at the Sun's history, *Science*, *247*, 39–44.

Raisbeck, G. M., and F. Yiou (2004), Comment on "Millennium scale sunspot number reconstruction: Evidence for an unusually active Sun since the 1940s", *Phys. Rev. Lett.*, *92*, 199001.

Raisbeck, G. M., F. Yiou, M. Fruneau, J. M. Loiseaux, M. Lieuvin, and J. C. Ravel (1981a), Cosmogenic ^{10}Be/^{7}Be as a probe of atmospheric transport processes, *Geophys. Res. Lett.*, *8*, 1015–1018.

Raisbeck, G. M., F. Yiou, M. Fruneau, J. M. Loiseaux, M. Lieuvin, J. C. Ravel, and C. Lorius (1981b), Cosmogenic ^{10}Be concentrations in Antarctic ice during the past 30,000 years, *Nature*, *292*, 825–826.

Raisbeck, G. M., F. Yiou, D. Bourles, C. Lorius, J. Jouzel, and N. I. Barkov (1987), Evidence for two intervals of enhanced ^{10}Be in Antarctic ice during the last glacial period, *Nature*, *326*, 273–277.

Rasch, P. J., et al. (2000), A comparison of scavenging and deposition processes in global models: Results from the WCCRP Cambridge Workshop of 1995, *Tellus, Ser. B*, *52*, doi:10.1034/j.1600-0889.2000.00980.

Rind, D., J. Lerner, K. Shah, and R. Suozzo (1999), Use of on-line tracers as a diagnostic tool in general circulation model development: 2. Transport between the troposphere and stratosphere, *J. Geophys. Res.*, *104*, 9151–9167.

Rind, D., P. Demenocal, G. L. Russell, S. Sheth, D. Collins, G. A. Schmidt, and J. Teller (2001a), Effects of glacial meltwater in the GISS Coupled Atmosphere-Ocean Model: 1. North Atlantic Deep Water response, *J. Geophys. Res.*, *106*, 27,335–27,354.

Rind, D., G. L. Russell, G. A. Schmidt, S. Sheth, D. Collins, P. Demenocal, and J. Teller (2001b), Effects of glacial meltwater in the GISS Coupled Atmosphere-Ocean Model: 2. A bi-polar seesaw in Atlantic Deep Water production, *J. Geophys. Res.*, *106*, 27,355–27,366.

Schmidt, G. A., et al. (2006), Present day atmospheric simulations using GISS Model-E: Comparison to in-situ, satellite and reanalysis data, *J. Clim.*, *19*, 153–192, doi:10.1175/JCLI3612.1.

Schwander, J., T. Sowers, J. M. Barnola, T. Blunier, A. Fuchs, and B. Malaize (1997), Age scale of the air in the summit ice: Implications for glacial-interglacial temperature changes, *J. Geophys. Res.*, *102*, 19,483–19,493.

Severinghaus, J. P., T. Sowers, E. J. Brook, R. B. Alley, and M. L. Bender (1998), Timing of abrupt climate change at the end of the Younger Dryas interval from thermally fractionated gases in polar ice, *Nature*, *391*, 141–146.

Shindell, D. T., D. Rind, N. Balachandran, J. Lean, and P. Lonergan (1999), Solar cycle variability, ozone, and climate, *Science*, *284*, 305–308.

Shindell, D. T., G. A. Schmidt, R. L. Miller, and M. E. Mann (2003), Volcanic and solar forcing of climate changes during the preindustrial era, *J. Clim.*, *16*, 4094–4107.

Steig, E. J., P. J. Polissar, M. Stuiver, P. M. Grootes, and R. C. Finkel (1996), Large amplitude solar modulation cycles of ^{10}Be in Antarctica: Implications for atmospheric mixing processes and interpretation of the ice core record, *Geophys. Res. Lett.*, *23*, 523–526.

Steig, E. J., E. J. Brook, J. W. C. White, C. M. Sucher, M. L. Bender, S. J. Lehman, D. L. Morse, E. D. Waddington, and G. D. Clow (1998), Synchronous climate changes in Antarctica and the North Atlantic, *Science*, *282*, 92–95.

Steig, E. J., D. L. Morse, E. D. Waddington, M. Stuiver, and P. M. Grootes (2000), Wisconsinan and Holocene climate history from an ice core at Taylor Dome, western Ross Embayment, Antarctica, *Geogr. Ann.*, *82*, 213–235.

Textor, C., et al. (2006), Analysis and quantification of the diversities of aerosol life cycles within AEROCOM, *Atmos. Chem. Phys.*, *6*, 1777–1813.

von Grafenstein, U., H. Erlenkeuser, J. Miller, J. Jouzel, and S. Johnsen (1998), The cold event 8200 years ago documented in oxygen isotope records of precipitation in Europe and Greenland, *Clim. Dyn.*, *14*, 73–81.

Willson, R. C., and H. S. Hudson (1988), Solar luminosity variations in solar cycle 21, *Nature*, *332*, 95–97.

Yiou, F., et al. (1997), Beryllium 10 in the Greenland Ice Core Project ice core at Summit, Greenland, *J. Geophys. Res.*, *102*, 26,783–26,794.

Zanis, P., et al. (2003), An estimate of the impact of stratosphere-to-troposphere transport (STT) on the lower free tropospheric ozone over the Alps using ^{10}Be and ^{7}Be measurements, *J. Geophys. Res.*, *108*(D12), 8520, doi:10.1029/2002JD002604.

C. V. Field, D. Koch, and G. A. Schmidt, NASA Goddard Institute for Space Studies, 2880 Broadway, New York, NY 10025, USA. (cfield@giss.nasa.gov)

C. Salyk, Division of Geological and Planetary Sciences, California Institute of Technology, 150-21, Pasadena, CA 91125, USA.